Available online at www.sciencedirect.com
SCIENCE DIRECT
Biochimica et Biophysica Acta 1757 (2006) 225–239
BIOCHIMICA ET BIOPHYSICA ACTA
BBA
http://www.elsevier.com/locate/bba

Review

Elucidating the mechanisms of coupled electron transfer and catalytic reactions by protein film voltammetry

Judy Hirst *

Medical Research Council Dunn Human Nutrition Unit, Wellcome Trust/MRC Building, Hills Road, Cambridge, CB2 2XY, UK

Received 1 February 2006; received in revised form 28 March 2006; accepted 1 April 2006
Available online 7 April 2006

Abstract

Protein film voltammetry, the direct electrochemistry of redox enzymes and proteins, provides precise and comprehensive information on complicated reaction mechanisms. By controlling the driving force for a reaction (using the applied potential) and monitoring the reaction in real time (using the current), it allows thermodynamic and kinetic information to be determined simultaneously. Two challenges are inherent to protein film voltammetry: (i) to adsorb the protein or enzyme in a native and active configuration on the electrode surface, and (ii) to understand and interpret voltammetric results on both a qualitative and quantitative level, allowing mechanistic models to be proposed and rigorous experiments to test these models to be devised. This review focuses on the second of these two challenges. It describes how to use protein film voltammetry to derive mechanistic and biochemically relevant information about redox proteins and enzymes, and how to evaluate and interpret voltammetric results. Selected key studies are described in detail, to illustrate their underlying principles, strategies and physical interpretations.

Keywords: Electrocatalysis; Electrochemistry; Protein film voltammetry; Coupled electron transfer; Redox protein

1. Introduction: protein film voltammetry

The direct electrochemistry of redox proteins and enzymes, protein film voltammetry, is becoming established as a method which is able to provide precise and comprehensive information on complicated reaction mechanisms [1–3]. In protein film voltammetry (PFV), the protein is adsorbed directly onto the electrode, removing the necessity for it to diffuse to the surface. This innovation was key to the development of protein electrochemistry [4], as protein diffusion (which is of no interest to the biochemist) is invariably slow and rate determining, obscuring all other more intriguing features. They include the thermodynamics and kinetics of coupled reactions and substrate transformations, in addition to reduction potentials.

Upon adsorbing to the electrode surface (see Scheme 1), it is crucial that the protein molecules retain their native structure and properties. This is easily confirmed for a redox enzyme because its catalytic properties should be retained. It is less easily confirmed for a non-catalytic redox protein, but one would hope that at least one property of the protein, such as the reduction potential or spectroscopic signature of a cofactor, may measured both in solution and on the electrode surface and compared [4]. Although large shifts in potential should not be tolerated without reason, reduction

Abbreviations: A, electrode area (cm^2); C*c*P, cytochrome *c* peroxidase; CV, cyclic voltammetry; *E*, applied potential (V); $E^{0'}$, reduction potential at pH 7 (V); $E_{1/2}$, reduction potential under non-standard conditions (V); E_x, $E_{1/2}$ for specified interconversion (V); E_{alk} or E_{acid}, pH independent reduction potential under alkaline or acid conditions (V); FAD, flavin adenine dinucleotide; *i*, current (A cm^{-2}); i_{lim}, limiting (potential independent) current; IET, interfacial electron transfer; *n*, number of electrons transferred; *m*, number of protons transferred; m_0, mass transport coefficient (cm s^{-1}); PFV, protein film voltammetry; PGE, pyrolytic graphite edge; S, substrate; S_B, substrate concentration in bulk solution; S_0, substrate concentration at the electrode surface; $W_{1/2}$, peak width at half height (V); Γ_X, surface concentration of species X (mol cm^{-2}); Γ_{Total}, total surface concentration (mol cm^{-2}); *v*, potential scan rate (V s^{-1})

* Tel.: +44 1223 252810; fax: +44 1223 252815.
E-mail address: jh@mrc-dunn.cam.ac.uk.

0005-2728/$ - see front matter © 2006 Elsevier B.V. All rights reserved.
doi:10.1016/j.bbabio.2006.04.002

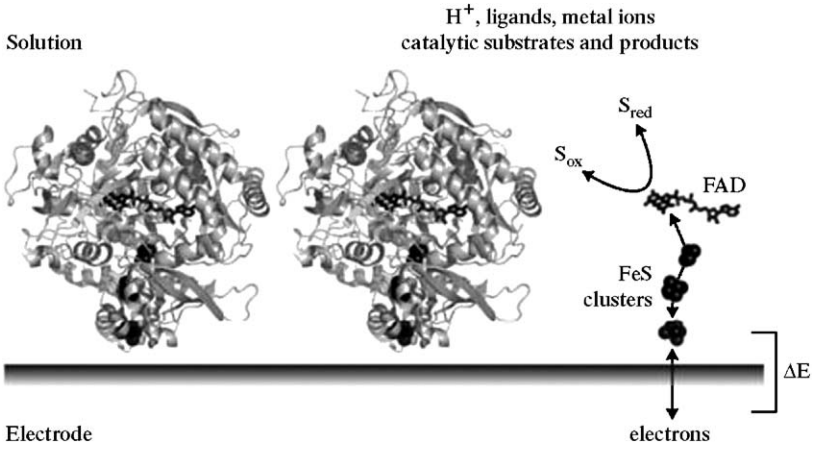

Scheme 1. Idealised representation of a protein film voltammetry experiment. An enzyme (in this case the hydrophilic domain of fumarate reductase from *Escherichia coli* [17]) is adsorbed on the electrode surface, with a chain of three iron–sulphur clusters connecting the electrode to the active site. Interfacial electron transfer (IET, between electrode and enzyme) is driven by the applied electrode potential (ΔE), and substrates access the catalytic site from solution. The enzyme's cofactors are also accessible to other solution phase species, for example, protons, ligands and metal ions.

potentials often do shift slightly upon adsorption (by 20 mV or so) reflecting the altered environment or the preferential adsorption of one oxidation state, and perturbations may be observed when the protein is adsorbed within a film of co-adsorbate because it is embedded within the electrical double layer [5]. In fact, for some proteins, the interfacial environment may actually be more relevant to the physiological situation than dilute solution. Of the many different electrode surfaces which have been investigated for their ability to adsorb a native protein, pyrolytic graphite edge (PGE) electrodes have had marked success [1–3,6]. This is probably because their surfaces are microscopically rough and chemically heterogeneous, allowing the protein a 'choice' of environment [7]. Consequently, PGE electrodes also have a number of disadvantages, such as potential dependent changes in surface chemistry, which may be avoided by more ideal (but less widely applicable) surfaces, such as organic monolayers on gold [8]. Although creating an appropriate interface for PFV is undoubtedly the first experimental challenge which must be overcome it has been discussed previously [4,5] and is not the focus of the current article.

A second important criterion is that at least one of the protein's redox cofactors must be in close proximity to the electrode surface (see Scheme 1) to form an electrical contact—so systems which succeed in PFV are often small proteins, or enzymes which transfer electrons to an external redox partner rather than those with deeply buried, insulated active sites. The shorter the distance between electrode and cofactor the faster electrons exchange between the two, and the better the chance that the process of interest is not dominated or obscured by interfacial electron transfer (IET) kinetics. The rate of IET increases with the thermodynamic driving force (set by the applied electrochemical potential) as described by several models of varying complexity and accuracy [9,10]. At the potentials applied in a typical PFV experiment the different models behave very similarly, thus, to allow this review to focus on determining biologically relevant information intrinsic to the protein, only the simplest model, the semi-empirical Butler–Volmer theory is described here.

Scheme 1 shows an idealised representation of a PFV experiment. Protein molecules adsorb to the electrode surface, in a native and electroactive configuration, to monolayer coverage or less. Consequently, PFV requires only very small amounts of sample. A typical monolayer film contains around 10^{-11} mol cm^{-2} (around 1 pmol on a standard electrode)—and some PFV experiments are possible with coverages which are significantly less than monolayer. Because the proteins form only a single layer their active sites are readily accessible to species in solution – protons, ligands, metal ions and catalytic substrates – allowing the study of *coupled* reactions. An added advantage of the protein film configuration is that the electrode can be switched between solutions of different composition and pH (an instant dialysis) allowing measurements under conditions in which the protein is only transiently stable. For example, Rieske cluster potentials can be measured at pH 14 by PFV [11]. The coupled reactions are the raison d'être of the electron transfer events, and it is because PFV has proved able to address both the thermodynamic and kinetic aspects of these reactions that it has come into its own as a powerful new technique in biochemistry.

This review aims to describe how to use PFV to derive mechanistic and biochemically interesting information about redox proteins and enzymes, and how to evaluate and interpret voltammetric results. Rather than attempting a comprehensive survey of the literature, selected key studies and the underlying principles of their experimental strategies and physical interpretations are described in detail.

2. Thermodynamic measurements: the reduction potential

The simplest protein film voltammetry experiment is the measurement of the reduction potentials of the cofactors in an enzyme or protein using cyclic voltammetry (Figs. 1 and 2). Cyclic voltammetry (CV) is the most commonly used electrochemical technique in PFV. Its main advantage is that it is relatively easy to evaluate the system's overall behaviour by inspection (reversible or not, coupled reaction or not, catalytically active or not…) and problems and artefacts are rapidly identified and diagnosed. A CV measurement is also quick and accurate. The electrochemical potential (*x*-axis) is varied linearly and repeatedly, between high and low potential limits, to drive the oxidation or reduction of the redox centres, and the transfer of electrons is monitored via the current (*y*-axis, reduction gives a negative current, oxidation gives a positive current). Thus, the CV experiment is interactive: it both induces and monitors the reaction.

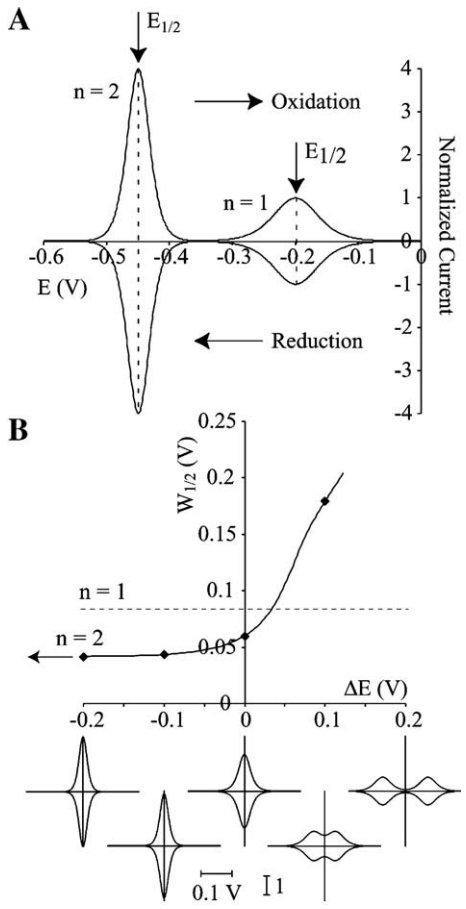

Fig. 1. Calculated voltammetric peaks from adsorbed proteins and enzymes in the absence of catalytic substrate. (A) Calculated waveshapes for one and two electron transfers, showing that the two electron cofactor produces sharper and narrower peaks (four times the height and half the width of the one electron cofactor). In both cases, the oxidative and reductive peaks are symmetrical and the peak separation is zero. (B) Variation of peak half-height width ($W_{1/2}$) for a cofactor which accepts two electrons sequentially ($\Delta E = E_{O/1} - E_{1/R}$), and calculated waveshapes for the different potential separations. The curve is terminated when the peak splits into two and the overall half-height width is no longer a meaningful parameter. In all cases $E_{AV}=0$, and all voltammograms calculated for 0 °C. The width of a single, one-electron peak is shown as a dashed line for comparison.

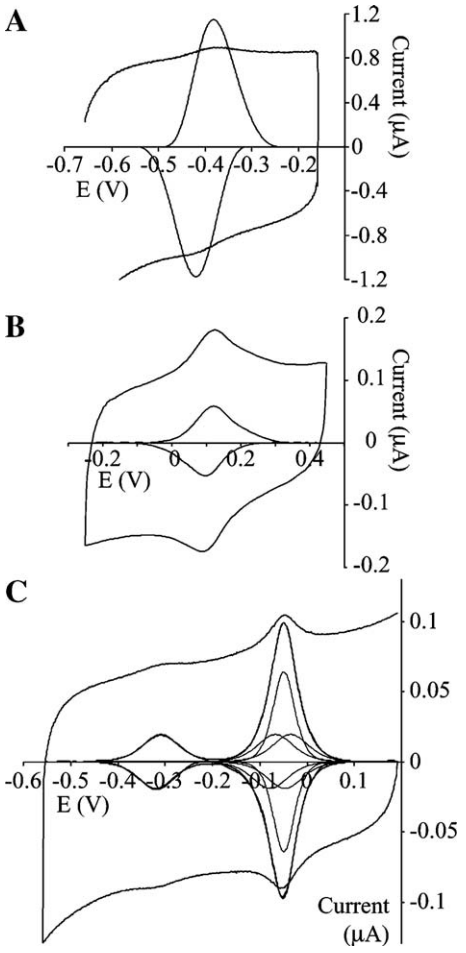

Fig. 2. Examples of experimentally recorded reversible voltammograms. (A) The [2Fe–2S] cluster in the over-expressed 24 kDa subunit from *Paracoccus denitrificans* complex I on a pyrolytic graphite edge electrode (10 mV s^{-1}, pH 5.3, 20 °C, peaks expanded) [16]. (B) Azurin from *Pseudomonas aeruginosa* on a gold electrode modified with decanethiol (3.6 V s^{-1}, pH 4, 0 °C), as described in [8]. (C) Fumarate reductase from *Escherichia coli* on a pyrolytic graphite edge electrode (10 mV s^{-1}, pH 7, 0 °C, peaks expanded). Deconvoluted signals from the FAD and three iron–sulphur clusters are also shown [70]. The data used to make panels B and C were provided by Prof. F. A. Armstrong, Oxford University.

If electron transfer (both between the protein and the electrode, and between different cofactors in the protein) is fast enough to maintain the redox level of the cofactors at close to equilibrium at every potential then the voltammogram is *reversible*, and displays symmetrical peak shapes and small peak-to-peak separations (ideally zero). The form of a reversible voltammogram is described by the Nernst equation (Eq. (1)) and by relating changes in Γ_{Red} to current (Eq. (2)) (see Fig. 1A) [12]. Because the protein film is comprised of a finite number of molecules the current drops to zero when the redox reaction is completed, and the area under the peak defines the number of molecules in the protein film. In contrast, the voltammetry of a soluble and

diffusing species maintains a current at high overpotential due to its continuous replenishment from bulk solution [10].

$$\frac{\Gamma_{\mathrm{Red}}}{\Gamma_{\mathrm{Total}}} = \frac{1}{e^{(E-E_{1/2})\mathrm{nF/RT}} + 1} \tag{1}$$

$$i = -\mathrm{nFA}v\frac{\mathrm{d}\Gamma_{\mathrm{Red}}}{\mathrm{d}E} = \frac{n^2F^2Av\Gamma_{\mathrm{Total}}}{\mathrm{RT}}\frac{e^{(E-E_{1/2})\mathrm{nF/RT}}}{[e^{(E-E_{1/2})\mathrm{nF/RT}} + 1]^2} \tag{2}$$

Experimentally, reversible voltammograms are obtained when the potential scan rate is slow relative to the rate of IET (and any coupled processes). Under these conditions, the peak potentials of both the oxidative and reductive peaks should be the same, and they are then equal to the reduction potential ($E_{1/2}$). In practice, a small peak separation (~20 mV) is often present [7] and the reduction potential is defined by the average of the two peak potentials (obviously $E_{1/2}$ cannot be defined if only one peak is present, as the system is not reversible). If the scan rate is too fast then IET cannot 'keep up' and the peaks separate and change in shape. In this situation their average potential may or may not be equal to $E_{1/2}$.

Fig. 1A shows two pairs of ideal signals, generated using Eq. (2)—from a one-electron cofactor such as an iron–sulphur cluster ($n=1$), and from a two-electron cofactor ($n=2$). Eq.(2) shows that the peak height depends on n^2, so that a two-electron cofactor has a four times higher peak, making it more easily distinguished from the background current and/or experimental noise. Calculation of the peak half-height width ($W_{1/2}$, the width of the peak measured at half its maximum height) shows that at 0 °C the theoretical $W_{1/2}$ for a one-electron peak is 83 mV and that of a two-electron peak is 41.5 mV (Eq. (3), calculated from Eq. (2) at $i=i_{\mathrm{Peak}}/2$). Thus, in principle, the n-value can be readily calculated from an experimental voltammogram. In practice, peaks are often broadened by thermodynamic dispersion, leading to $W_{1/2}$ values greater than otherwise predicted.

$$W_{1/2} = \frac{2RT}{nF}\ln\left(3+2\sqrt{2}\right) \tag{3}$$

However, pure $n=2$ waveshapes are rarely (if ever) observed, since $n=2$ implies that the intermediate (radical) state of the cofactor never exists. For example, flavins are two-electron cofactors but their semiflavin states display a wide range of stability [13]. Therefore, the reduction of a flavin must be considered as two consecutive one-electron events. Eq. (4) is the Nernst equation which describes the surface populations of the three oxidation states (fully reduced (Γ_{R}), semi-reduced intermediate (Γ_{I}), and oxidised (Γ_{O})) as a function of potential [14].

$$E = E_{\mathrm{O/I}} - \frac{\mathrm{RT}}{F}\ln\left\{\frac{\Gamma_{\mathrm{I}}}{\Gamma_{\mathrm{O}}}\right\} = E_{\mathrm{I/R}} - \frac{\mathrm{RT}}{F}\ln\left\{\frac{\Gamma_{\mathrm{R}}}{\Gamma_{\mathrm{I}}}\right\} \tag{4}$$

Eq. (4) can be used to calculate voltammetric waveshapes by replacing $\mathrm{d}\Gamma_{\mathrm{Red}}$ in Eq. (2) by $\mathrm{d}\{2\Gamma_{\mathrm{R}}+\Gamma_{\mathrm{I}}\}$ and Fig. 1B shows a set of examples from a range of values of ΔE ($=E_{\mathrm{O/I}}-E_{\mathrm{I/R}}$). At $\Delta E=0.2$ V the peakshape is composed of two individual peaks as the radical is stable. At $\Delta E=-0.2$ V the radical is very unstable (addition of the second electron is more favourable than the first), and the waveshape is close to that for an $n=2$ process. At intermediate ΔE values a single broad peak is observed. The relationship between ΔE and $W_{1/2}$ (Fig. 1B) shows that, in principle, it is possible to determine both $E_{\mathrm{O/I}}$ and $E_{\mathrm{I/R}}$ from a single voltammogram (provided that the limit at $\Delta E<<0$ has not been reached). Note that an analytical solution for $W_{1/2}$ as a function of ΔE has been derived [15].

Fig. 2 shows representative experimental voltammograms. In Fig. 2A, a $[2\mathrm{Fe}–2\mathrm{S}]^{2+/1+}$ cluster in an over-expressed ferredoxin is reversibly oxidised and reduced on a PGE electrode [16]. The background subtracted signals (from which the electrode capacitance has been removed) show that the peaks are symmetrical and close together. Fig. 2B displays the $\mathrm{Cu}^{2+/1+}$ transition in the blue copper protein azurin, adsorbed on a gold electrode modified with decanethiol [8]. Fig. 2C shows a voltammogram from the hydrophilic domain of fumarate reductase from *Escherichia coli* [17] adsorbed on a PGE electrode. The sharp, intense signal from the two-electron FAD cofactor stands out above the signals from three ($n=1$) iron–sulphur clusters, and the quality of the data allows the envelope of signals at ca. −0.05 V to be deconvoluted to reveal the component contributions [15,18,19].

In principle, every biological redox cofactor is accessible to study by PFV. Examples of those which have been characterised by CV include iron–sulphur clusters [20–22], copper centres [23–25] molybdenum centres [26,27], haems [28–31] and flavins [18,30]. In a number of cases redox states at unusually low or high potentials have been characterised, including the all-ferrous [3Fe–4S] (−0.4 to −0.8 V) [32] and Rieske [2Fe–2S] (−0.6 to − 0.9 V) [33] clusters at low potential, and compound I in cytochrome *c* peroxidase (C*c*P) at high potential (~+0.75 V) [28]. Thus, PFV is versatile in both the cofactors which may be studied, and the potential range over which they may be studied.

3. Thermodynamic measurements: square schemes and the detection of coupled reactions

The mechanistic information gained from measurement of a single reduction potential is fundamental but limited—coupled reactions are the ultimate reason for the electron transfer event and are of fundamental biological importance, most obviously in complex energy transducing respiratory and photosynthetic enzymes. PFV is ideally suited to the identification of coupled reactions because each PFV experiment requires only a few minutes and so the effects of an experimental variable on the reduction potential can be evaluated very rapidly (a whole pH dependence in one afternoon). Importantly, each measurement must still be carried out under reversible conditions, in which both the electrochemical and chemical reactions are maintained at close to equilibrium. Coupled reactions occur because of a change in oxidation state, and include ligand, substrate and proton binding and conformational changes. They contribute thermodynamically to the redox process, and how they affect

the reduction potential is illustrated most clearly by using one or more thermodynamic square schemes. Square schemes define the appropriate thermodynamic parameters, such as binding constants and pK values (specific to particular oxidation states), and reduction potentials (specific to particular chemical species).

3.1. Redox-state dependent protonation of Rieske [2Fe–2S] clusters

Fig. 3A shows how the reduction potential of the Rieske cluster in the soluble Rieske domain from the bovine cytochrome bc_1 complex varies with pH [11,34]. Rieske clusters form part of the mechanism of quinol oxidation at the Q_O site in cytochrome bc_1 complexes—they may accept both an electron and a proton upon quinol oxidation and thus play a key role in energy transduction [35]. In Rieske clusters, one of the iron centres is coordinated by two histidine ligands, which deprotonate at high pH. In Fig. 3A, the gradient of the curve varies from zero at low pH, to ~60 mV per decade, to ~120 mV per decade, to zero again at high pH. The Rieske cluster is an $n=1$ couple, and so it is immediately apparent from the Nernst equation (Eq. (5)) that these gradients correspond to regions of pH in which 0, 1 or 2 (m) protons are transferred upon oxidation or reduction.

$$\mathrm{Ox} + \mathrm{ne}^- + m\mathrm{H}^+ \Leftrightarrow \mathrm{Red}$$
$$E_{1/2} = E^{0'} - \frac{m\mathrm{RT}\ln(10)}{\mathrm{nF}}(\mathrm{pH} - 7) \quad (5)$$

Consequently, the square schemes shown in Fig. 3A describe completely the coupled transfer of up to two protons. They comprise two 'fundamental' reduction potentials (at the low and high pH limits) and four pK values (one for each proton, in each oxidation state), and may be used to derive a Nernst equation (Eq. (9)) to fit the data over the entire pH range. The derivation (Eq. (6)–(9)) is presented for reference:

$$E = E_{\mathrm{alk}} - \frac{\mathrm{RT}}{F}\ln\left[\frac{\Gamma_{\mathrm{Red}}}{\Gamma_{\mathrm{Ox}}}\right] \quad (6)$$

$$\Gamma_{\mathrm{Ox}} + \Gamma_{\mathrm{Ox-H^+}} + \Gamma_{\mathrm{Ox-2H^+}} = \Gamma_{\mathrm{Ox}}\left(1 + \frac{[\mathrm{H}^+]}{K_{\mathrm{Ox2}}}\left(1 + \frac{[\mathrm{H}^+]}{K_{\mathrm{Ox1}}}\right)\right) \quad (7)$$

by substitution of Eq. (7), and its equivalent for the reduced species, into Eq. (6):

$$E = E_{\mathrm{alk}} - \frac{\mathrm{RT}}{F}\ln\left[\left\{\frac{\Gamma_{\mathrm{Red}} + \Gamma_{\mathrm{Red-H^+}} + \Gamma_{\mathrm{Red-2H^+}}}{\Gamma_{\mathrm{Ox}} + \Gamma_{\mathrm{Ox-H^+}} + \Gamma_{\mathrm{Ox-2H^+}}}\right\} \times \left\{\frac{1 + ([\mathrm{H}^+]/K_{\mathrm{Ox2}})(1 + [\mathrm{H}^+]/K_{\mathrm{Ox1}})}{1 + ([\mathrm{H}^+]/K_{\mathrm{Red2}})(1 + [\mathrm{H}^+]/K_{\mathrm{Red1}})}\right\}\right] \quad (8)$$

When the sum of reduced species is equal to the sum of the oxidised species then $E=E_{1/2}$ and

$$E_{1/2} = E_{\mathrm{alk}} - \frac{\mathrm{RT}}{F}\ln\left[\left(1 + \frac{[\mathrm{H}^+]}{K_{\mathrm{Ox2}}} + \frac{[\mathrm{H}^+]^2}{K_{\mathrm{Ox1}}K_{\mathrm{Ox2}}}\right) \div \left(1 + \frac{[\mathrm{H}^+]}{K_{\mathrm{Red2}}} + \frac{[\mathrm{H}^+]^2}{K_{\mathrm{Red1}}K_{\mathrm{Red2}}}\right)\right] \quad (9)$$

Obviously, equivalent equations may be derived for any such thermodynamic scheme. The data in Fig. 3A have been fit using Eq. (9), with pK_{Ox1}=7.55, pK_{Ox2}=9.10, pK_{Red1}=11.8, pK_{Red2}=12.8, E_{acid}=+0.31 V, E_{alk}=−0.15 V. As expected, the proton binds most strongly to the reduced states, and the protonated cluster is the easiest to reduce [11]. Similar experiments have been used to characterise the reduction potentials of different Rieske clusters (which all show the same basic pH-dependence), and to investigate the effects of specific

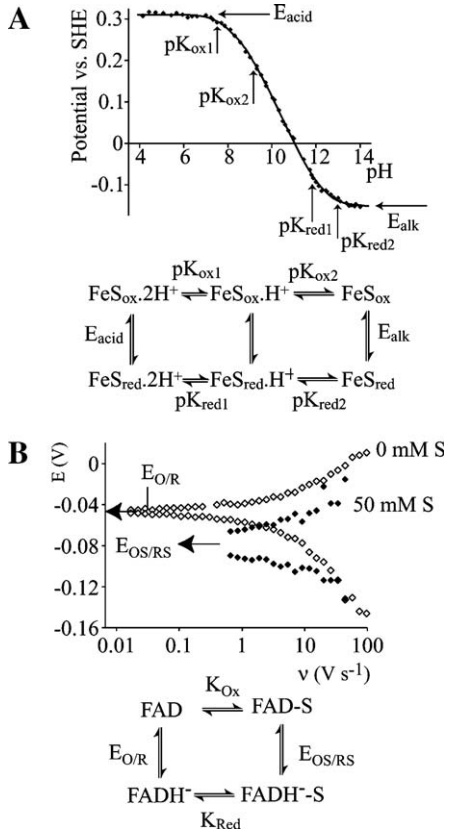

Fig. 3. The application of thermodynamic square schemes to interpreting variations in reduction potential. (A) The pH dependence of the reduction potential of the Rieske [2Fe–2S] cluster from the over-expressed soluble domain of the protein from the bovine cytochrome bc_1 complex, and the corresponding set of square schemes [11,22,34]. (B) Plot of the reductive and oxidative peaks for the FAD cofactor in fumarate reductase from *E. coli*, in the presence and absence of a substrate, succinate, as a function of the potential scan rate (ν). In the absence of succinate, the FAD potential is the average peak potential. In the presence of 50 mM succinate fast potential scan rates outrun catalysis and, because the average peak potential is scan-rate independent, it defines the potential of the enzyme–substrate complex [41]. The data used to make Figure B were provided by Prof. F. A. Armstrong, Oxford University.

nearby residues [22,34,36]. They have been applied previously to many other coupled reactions, including coupled proton-electron transfer at [3Fe–4S] clusters [32,37,38], flavins [18,30], and a molybdenum centre [27].

3.2. Detection and thermodynamic characterisation of a short-lived catalytic intermediate: a Michaelis complex

It is not possible to measure the reduction potential of a short-lived intermediate by conventional means (such as a redox titration), or by reversible voltammetry. However, a 'transient' reduction potential may often be the mechanistically relevant value for a physiological electron transfer event —which does not occur at equilibrium or when the system has been allowed to completely relax [39]. Providing that IET is facile, fast scan PFV experiments provide access to the transient value [40]. In Fig. 3B [41], the open symbols show how the oxidative and reductive peaks for the FAD in the active site of fumarate reductase from *E. coli* separate symmetrically about the reduction potential as the scan rate is increased. The separation is a function of the scan rate and the rate of IET, and the peaks separate because IET is not fast enough to maintain a Nernstian equilibrium and so the redox state of the protein 'lags behind' the set potential. Because the peaks separate symmetrically they are considered as a simple electron transfer reaction (any coupled reactions are fast enough that they do not influence the rate of the redox process) and so their average potential can be equated to the reduction potential. The closed symbols show equivalent results recorded in the presence of 50 mM succinate. At the start of the experiment the FAD is reduced, and a high concentration of succinate is present to occupy the binding site (ca. 90% occupied). The reduced FAD cannot react with succinate, but as the potential is scanned to positive potentials the FAD is oxidised, and the reactive 'Michaelis' complex is formed. At slow scan rates, it reacts to form products, but at fast scan rates the slow reaction with succinate (the physiological product) is outrun and the complex is re-reduced to its original, non-reactive state. When the scan-rate is fast enough to outrun the catalytic reaction the peaks separate symmetrically about the reduction potential of the Michaelis complex. The corresponding thermodynamic square is shown in Fig. 3B and leads to Eq. (10) because the sum of all the free-energy changes (ΔG) must equal zero:

$$RT ln K_{Ox} - 2FE_{OS/RS} - RT ln K_{Red} + 2FE_{O/R} = 0 \qquad (10)$$

Therefore, the difference between the two reduction potentials (±succinate) relates directly to the difference in the binding constants of succinate to the oxidised and reduced FAD. Similar experiments carried out for fumarate binding to the active site of flavocytochrome c_3 from *Shewanella frigidimarina* showed that fumarate binds with approximately the same affinity, regardless of the oxidation state of the FAD [42]. At present the generality of these observations, from two different fumarate reductase enzymes, has not been established, but the implication that succinate (the reduced product) may bind more tightly to the oxidised FAD (Eq. (10)), whereas fumarate (the reactant) is not selective, has obvious significance for the energetics of the catalytic reaction. Similar experiments have been applied to binding of an exogenous thiolate ligand to a [4Fe–4S] cluster [43] and to elucidating the role of a histidine ligand to the copper centre in azurin [23].

4. The kinetics of coupled reactions

Coupled reactions occur because of a change in oxidation state, and so the tight control under which the applied potential is held in a PFV experiment provides a huge advantage in deconvoluting the mechanisms of these reactions. In some cases, inspection of a set of consecutively recorded voltammograms shows clearly that a coupled reaction is occurring, because one set of peaks transform into another. For example, application of an oxidising potential to *Clostridium pasteurianum* ferredoxin causes expulsion of Fe^{2+} from one of the [4Fe–4S] clusters and turns the pair of peaks associated with that [4Fe–4S] cluster into the two pairs of peaks which are diagnostic of a [3Fe–4S] cluster [44]. In the opposite reaction, addition of various divalent metal ions such as Fe^{2+}, Zn^{2+}, Co^{2+} to the [3Fe–4S] containing *Desulfovibrio africanus* ferredoxin III converts [3Fe–4S] to [M3Fe–4S], and the reaction is visualised as one set of peaks convert gradually to another [20,45]. Such reactions are well defined and easily visualised in the PFV experiment, but appear unnecessarily complicated in solution experiments which exert no control over the potential domain.

By controlling both the potential and time domains of an experiment, PFV is capable of quantifying both the thermodynamics and kinetics of coupled reactions, and of deconvoluting complex mechanisms which occur on fast timescales. Perhaps the best example is coupled proton transfer to the [3Fe–4S] cluster in *Azotobacter vinelandii* ferredoxin I (*Av*FdI) (see Fig. 4) [46,47]. This system comprises a 'proton-transferring module' in which a carboxylate residue acts as a proton courier, enabling long-range, electron-coupled proton transfer from solvent to a buried cofactor. The simplicity of the system has allowed it to be characterised both thermodynamically and kinetically in exquisite detail, revealing how similar modules may operate in complex proton pumping enzymes, such as cytochrome *c* oxidase [47].

The thermodynamic scheme for coupled electron-proton transfer to the buried [3Fe–4S] cluster, derived from the dependence of reduction potential on pH, is presented in Fig. 4A [37,38]. For wild-type *Av*FdI E_{alk} is −0.44 V and pK_{red} is 7.8 ($E_{1/2}$ is pH independent above pH ~8.0, and pH dependent (Eq. (5)) below pH ~7.5). Fig. 4C shows how voltammetric peak positions depend on scan rate at $pH >> pK$, when electron transfer is uncoupled, along with representative voltammetric peaks [46]. The peaks separate symmetrically about E_{alk}, and their peak positions may be modelled using the Butler–Volmer equation, Eq. (11) (assuming that the transfer coefficient, $\alpha = 0.5$ [10]), to give

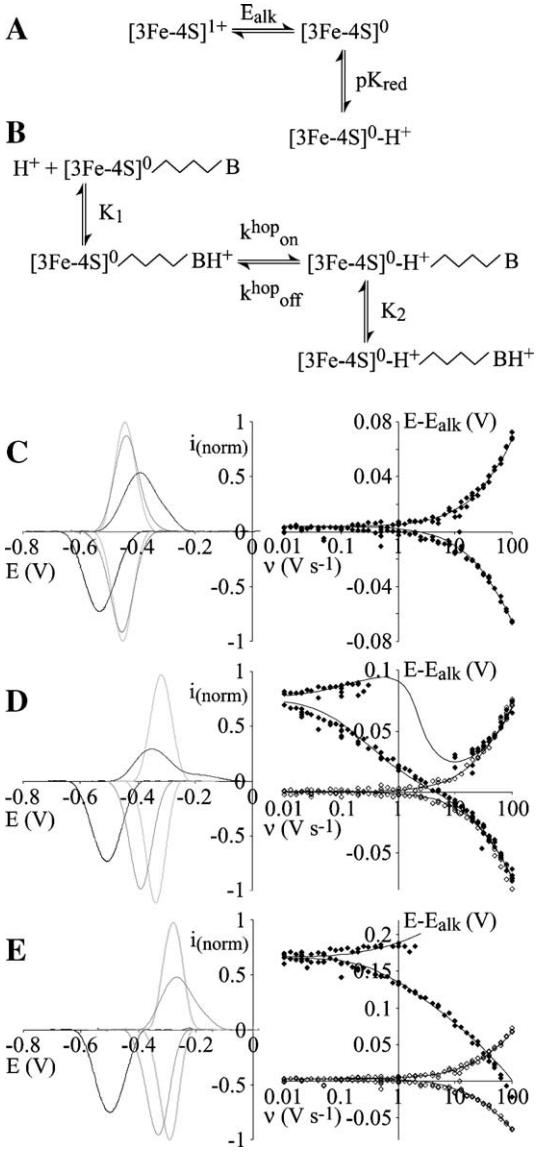

Fig. 4. Determination of the mechanism of coupled electron proton transfer to the [3Fe–4S] cluster in *Azotobacter vinelandii* ferredoxin I (*Av*FdI) using fast-scan protein film voltammetry [46]. (A) Thermodynamic scheme showing how the reduction potential varies as a function of pH. At high pH the reduction potential is E_{alk}, as electron transfer is uncoupled. At low pH (pH<<p*K*) the reduced cluster is protonated and the reduction potential is pH dependent. At intermediate pH the reduced cluster exists as a mixture of protonated and unprotonated species. (B) Reaction scheme for transfer of the proton across a hydrophobic barrier from a surface aspartate residue (B) to the cluster. The reaction involves rapid, pre-equilibrium protonation of the aspartate (K_1), reversible transfer across the barrier (k^{hop}_{on}, k^{hop}_{off}), and re-establishment of a protonation equilibrium for the aspartate (K_2). (C) Data recorded for *Av*FdI at pH>>p*K* (pH 8.55). The peaks separate symmetrically about the reduction potential as the scan rate is increased and the peak positions (♦) are modelled using the Butler–Volmer equation. Light grey, 0.01 V s^{-1}; grey, 1 V s^{-1}; black, 100 V s^{-1}. (D) Data recorded for the D15N mutant of *Av*FdI at pH<p*K* (pH 5.50). Electron transfer is coupled to protonation so that the peaks do not separate symmetrically. Light grey, 0.01 V s^{-1}; grey, 1 V s^{-1}; black, 100 V s^{-1}. The peak positions (♦) are modelled using the Butler–Volmer equation and the reaction scheme shown in (A), and the peak positions recorded at high pH are overlaid (◇). (E) Voltammograms recorded for *Av*FdI at pH<p*K* (pH 4.59). Again, electron transfer is coupled to protonation and the peaks do not separate symmetrically. Light grey, 0.01 V s^{-1}; grey, 1 V s^{-1}; black, 100 V s^{-1}. The peak positions (♦) are modelled using the Butler–Volmer equation and the reaction scheme shown in (B), and the peak positions recorded at high pH are overlaid (◇).

the modelled lines included in Fig. 4C.

$$k_{OX} = k_0 \exp\left(\frac{nF}{2RT}(E - E_{alk})\right)$$
$$k_{red} = k_0 \exp\left(-\frac{nF}{2RT}(E - E_{alk})\right) \quad (11)$$

No analytical solution for peak position as a function of scan rate exists, so the calculation requires a 'finite difference' approach. The initial concentration of each species is set (e.g. $\Gamma_{ox}=1$, $\Gamma_{red}=0$ at $E>>E_{alk}$) and then a small step is taken in potential, and the corresponding changes in Γ_{ox} and Γ_{red} are calculated. Γ_{ox} and Γ_{red} are adjusted, and the simulation proceeds across the potential range. If the steps are small enough the simulation 'converges' to the analogue limit — the true solution obtained when the potential steps are infinitely small. Experimental observables such as peak position and width are then calculated, and the best fit to the data is found by adjusting k_0 (Eq. (11)) [7,46]. For *Av*FdI k_0 is 600 s^{-1}, sufficient to allow the relatively fast coupled reactions described below to be characterised.

The carboxylate residue which carries the proton across the hydrophobic barrier in *Av*FdI is asp-15, and proton transfer is significantly retarded in the D15N mutant [37,38]. In Fig. 4D data from *Av*FdI–D15N are presented for pH<pK_{red}, and have been fitted using finite difference simulation of the scheme in Fig. 4A [46]. Data were recorded over a range of pH values, and could all be fit well using a single set of parameters: E_{alk}= −0.408 V, k_0=550 s^{-1}, pK_{red}=6.9 and k_{off}=2.5 s^{-1}. At pH<pK_{red} (Fig. 4D) reduction is coupled thermodynamically to cluster protonation: at slow scan rate an electron and a proton are transferred reversibly (the peaks are symmetrical and their separation is small); at intermediate scan rates protonation follows reduction (the reductive peak is sharp), but cluster deprotonation (which must precede oxidation) is outrun (the oxidative peak is severely broadened and unresolved); at the highest scan rates cluster protonation is outrun also (provided the scan is initiated at high potential) and the voltammetry mirrors that recorded at high pH. Thus, for the D15N mutant, the mechanism is relatively simple, and the voltammetric data can be characterised accurately over all available time domains.

In wild-type *Av*FdI asp-15 mediates proton transfer across the hydrophobic protein barrier, from solvent to cluster, providing much faster proton transfer kinetics than in *Av*FdI–D15N, but requiring a more complex mechanism. Fig. 4E displays the behaviour of wild-type *Av*FdI at low pH [46], and incorporates the fit from the mechanism shown in Fig. 4B. The mechanism comprises protonation of the surface residue D15 (pK_1=7.2), motion of the protonated aspartate headgroup into the protein and delivery of the proton to the reduced cluster (k^{hop}_{on}=1300 s^{-1} and k^{hop}_{off}=330 s^{-1}) and re-equilibration of the aspartate protonation state with the solution (pK_2=5.9). Cluster deprotonation follows the equivalent reverse mechanism, initiated by motion of the deprotonated aspartate toward the protonated cluster. Finally, note that although PFV was crucial in elucidating the mechanism of proton transfer, a complete molecular description was only possible by

combining PFV with structural analysis, site-directed mutagenesis and molecular dynamics simulations [47].

5. Catalytic voltammetry: thermodynamic control

In the presence of a catalytic substrate an adsorbed enzyme catalyses the redox transformation of substrate into product, and the electrode acts as a redox partner, transferring electrons to regenerate the active oxidation state of the active site. This process links the catalytic rate directly to the observed current, and allows the mechanism of catalysis to be interrogated in the potential domain. Fig. 5A shows calculated voltammograms to illustrate the principle. In the absence of substrate, Ox and Red interconvert reversibly according to the applied potential. When substrate is added it reacts with Ox to generate Red, and (assuming the potential is high enough) the electrode reaction then regenerates Ox, which can react again—and so on. Studies of catalysis by CV are typically carried out under the assumption that a steady-state is attained: the potential scan rate is low enough that each catalytic intermediate, or substrate or product concentration, is at steady-state at every potential (its rate of accumulation equals its rate of depletion). The observable criterion for steady-state is that decreasing the scan rate does not affect the catalytic voltammogram, and if the potential scan is halted then the catalytic current does not change. Scheme 2A illustrates the main processes which may limit the rate of

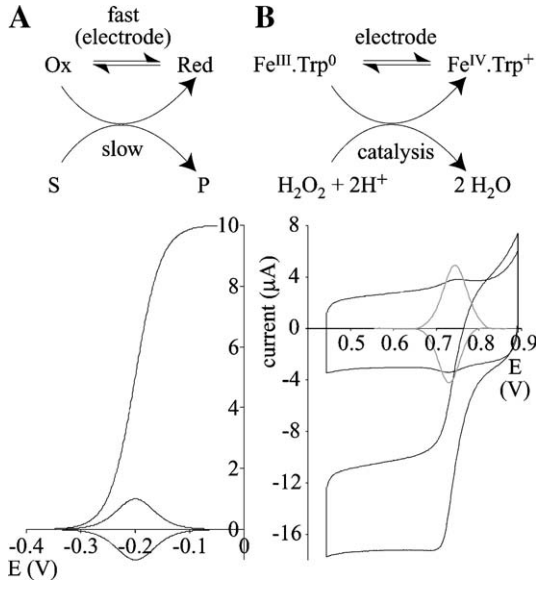

Fig. 5. Conversion of reversible oxidation and reduction of an adsorbed enzyme active site into catalytic turnover upon addition of substrate. (A) Calculated voltammograms showing how the reversible peaks from a one-electron redox couple convert to a sigmoidal one-electron wave upon addition of substrate. (B) Voltammograms from yeast C*c*P in the absence and presence of substrate [28]. The two peaks produced in the absence of substrate correspond to the two-electron oxidation and reduction of the enzyme (conversion of the haem Fe^{III} to Fe^{IV}, and oxidation of a tryptophan residue). On addition of H_2O_2 the enzyme is oxidised chemically and reduced electrochemically, resulting in a continuous flow of electrons from electrode to enzyme (a reductive current). The catalytic wave occurs at the same potential as the reversible redox peaks. Conditions: pH 6.1, 4 °C, 20 μM H_2O_2, 20 mV s^{-1}, 400 rpm. The data used to make panel B were provided by Prof. F. A. Armstrong, Oxford University.

electrocatalysis by an adsorbed enzyme. They comprise mass transport (the supply of substrate and the dispersal of product), the intrinsic enzyme kinetics, and IET.

If IET and mass transport are both much faster than the catalytic reaction then the catalytic current simply reflects the Nernstian pre-equilibrium population of the reactive oxidation state of the enzyme, 'amplified' by the catalytic transformation. This is an unusual, but simple situation, and is most likely (enzyme kinetics allowing) when mass transport is assisted by 'stirring' the solution—typically, a rotating disc electrode is used to provide a mathematically calculable rate of substrate supply to the surface. Fig. 5B shows the example of C*c*P [28]. In the absence of substrate a pair of peaks from the two-electron oxidation and reduction of the active site (haem Fe^{III}/Fe^{IV} and Trp^0/Trp^+) are evident. Upon the addition of H_2O_2 the $Fe^{III}.Trp^0$ state reacts chemically to form the Fe^{IV}/Trp^+ state, and is then regenerated by the electrode. Thus, the catalytic current follows the expected population of Fe^{III}/Trp^0 as a function of potential, so the catalytic voltammogram is sigmoidal, with the 'limiting current' (i_{lim}) imposed by the rate of enzyme turnover. Importantly, the catalytic wave confirms that the enzyme is adsorbed in a catalytically competent (native) state, and because the non-turnover and turnover potentials are close together, the non-turnover signals are confirmed as pertinent to the catalytic reaction.

For fumarate reductase from *E. coli* the catalytic oxidation of succinate (the physiological product) is sufficiently slow that catalytic turnover can be used to 'redox titrate' the FAD active site in varying substrate concentrations and pHs, to characterise its coupled electron transfer reactions, and to map out the energetic 'landscape' of catalytic turnover [41]. Fig. 6A shows background subtracted voltammograms recorded over a range of succinate concentrations, and Fig. 6C compares the normalised data (i/i_{lim}, where i_{lim} is the potential independent current at high overpotential) to normalised voltammograms calculated using the scheme in Fig. 6B. The population of each species in the pre-equilibrium can be calculated as a function of potential from the Nernst equations for each oxidised and reduced pair, expressions for the three dissociation constants, and by summing all species to 1 (Eq. (12) for OxS), and the normalised current follows from multiplying Γ_{OxS} by k_2, and dividing by the value at maximum overpotential.

$$\Gamma_{OxS} = \frac{[succ]}{K_O} \Bigg/ \left[1 + \frac{[succ]}{K_O} + \varepsilon_{O/I} \times \left(1 + \frac{[succ]}{K_I} + \varepsilon_{I/R}\left(1 + \frac{[succ]}{K_R}\right)\right)\right]$$
$$\text{where } \varepsilon_i = e^{\left\{(E_i - E)\frac{F}{RT}\right\}} \qquad (12)$$

In this way, by using catalysis to amplify the signal and so facilitate the redox titration, substrate dissociation constants were measured for each oxidation state of the FAD, and the two one-electron FAD potentials were calculated. Thus the influence of substrate on active site potential, and on the stability of the semiflavin radical, was determined.

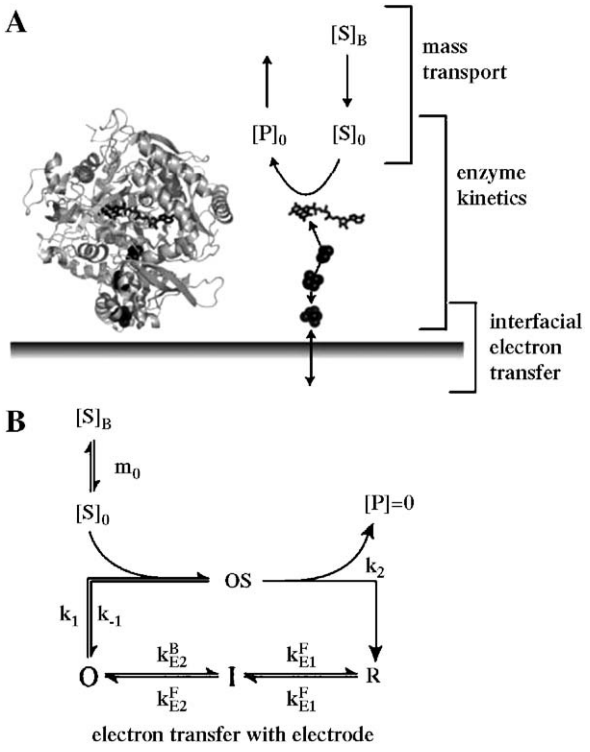

Scheme 2. The processes which may determine the rate of catalysis by an adsorbed enzyme. Mass transport (described by the parameter m_0) supplies catalytic substrate to the surface bound enzyme, and removes product. The enzyme kinetics comprise substrate binding, the catalytic transformation, product release, and any other such processes. They are often described by the Michaelis–Menten equation (by K_M and k_2), though they do not usually obey Michaelis–Menten kinetics. Interfacial electron transfer (IET) is the process of transferring electrons between electrode and enzyme, and may be described by a number of models (see text). Scheme 2B shows a basic mechanism for an enzyme catalysing a two-electron substrate oxidation reaction. $[S]_0$ is the substrate concentration at the electrode surface, and $[S]_B$ that in bulk solution. O, I and R are the oxidised, intermediate, and reduced states of the enzyme active site, and OS is the enzyme substrate complex.

Importantly, note that this approach is only possible when (i) mass transport is not limiting and (ii) k_2 is much smaller than the rates at which all associated equilibria (notably IET and substrate binding) are established. Therefore, it is unlikely to be widely applicable.

Finally, it is important to remember that an enzyme cannot catalyse a reaction that is thermodynamically forbidden (substrate reduction cannot occur substantially above the substrate reduction potential, and oxidation cannot happen substantially below it). When the enzyme potential is significantly higher than the substrate potential then the enzyme is able to catalyse substrate oxidation, not reduction, and vice versa. When the enzyme and substrate potentials are well matched the enzyme is able to catalyse the reaction efficiently in both directions, for example in the cases of mitochondrial succinate dehydrogenase [48] and NADH dehydrogenase [49]. In these cases, the presence of both oxidised and reduced substrates traces out voltammetric 'isosbestic points' of zero net current, which equate to the substrate's reduction potential. All potentials positive of these points correspond to substrate oxidation, all potentials negative correspond to substrate reduction. The difference between the potentials of the enzyme and the substrate determines how efficient the oxidative and reductive reactions are, relative to one another [48,50].

6. Catalytic voltammetry: characterising the kinetics

The simplest situation in which kinetic control by the enzyme is visualised is when sufficient overpotential is applied to drive the reaction at a rate that is independent of potential (i_{lim}). This happens (i) when, thermodynamically, the active site exists completely in its reactive oxidation state, and (ii) because the rate of IET increases rapidly with potential, so that at high driving force the 'regeneration' of the active site does not affect the overall rate. Ideally, i_{lim} can be defined at an overpotential of around 200 mV beyond the apparent

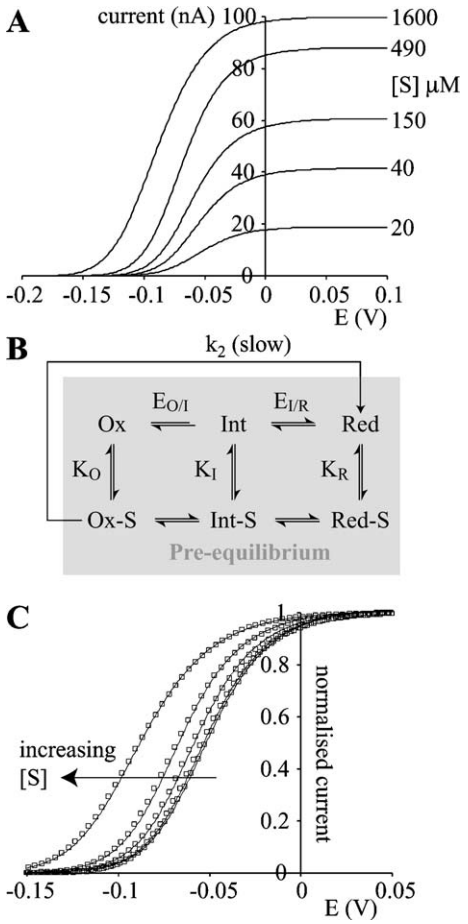

Fig. 6. Interpretation of succinate oxidation by fumarate reductase from *E. coli* using a pre-equilibrium model [41]. (A) Variation of the catalytic voltammograms with substrate concentration (background subtracted), pH 7.5, 1 mV s^{-1}, 3000 rpm, 20 °C. (B) Reaction scheme for succinate oxidation by fumarate reductase. Species within the grey box are established in a pre-equilibrium, such that the rate of substrate conversion is k_2 multiplied by the population of Ox–S. C). Data from panel A normalised to i_{lim} (open boxes), and compared to the predictions from the scheme using K_O=0.18 mM, K_I=0.63 mM, K_R=9 mM, $E_{O/I}$=− 0.066 V and $E_{O/R}$=− 0.059 V. The data used to make panels A and C were provided by Prof. F. A. Armstrong, Oxford University.

midpoint potential (see Fig. 5), and a requirement for excessive overpotential indicates that IET is either slow or complex (see below). Identification of the factors which are determinants of i_{lim} (see Scheme 2A) is possible by variation of the experimental conditions, in ways analogous to those implemented in conventional enzyme or electrochemical experiments. Typically, substrate supply to the surface is controlled by rotating the electrode, and so the concentration which the enzyme experiences is a function of bulk substrate concentration, electrode rotation rate, and the rate of depletion. The current expected if substrate supply is completely rate determining is given by the Levich equation (Eq. (13)) [10], where $S_0 \rightarrow 0$.

$$i_{Lev} = 0.620nFAD^{2/3}\omega^{1/2}\nu^{-1/6}\{S_B - S_0\} = nFAm_0\{S_B - S_0\} \quad (13)$$

D is the substrate diffusion coefficient ($cm^2\ s^{-1}$), ω is the electrode angular rotation rate (s^{-1}), ν is the kinematic viscosity (0.01 $cm^2\ s^{-1}$ at 20 °C), S_B and S_0 are the bulk and surface substrate concentrations, and m_0 is the mass transport coefficient.

If substrate supply is much faster than enzyme turnover then i_{lim} is determined by the enzyme kinetics, most simply by the Michaelis–Menten equation (Eq. (14)) [51].

$$\text{Rate} = \frac{\Gamma_{Total}k_2[S]}{K_M + [S]} \text{ where } K_M = \frac{k_2 + k_{-1}}{k_1} \quad (14)$$

In a typical electrochemical experiment, however, mass transport and enzyme kinetics are convoluted, because a steady-state concentration of substrate at the electrode surface is established between depletion by the enzyme and replenishment by mass transport. As the rate of mass transport increases $S_0 \rightarrow S_B$, and so i_{lim} at infinite rotation rate, as a function of S_B, can be used to estimate the kinetic parameters. Koutecky–Levich analysis uses plots of 1/current against 1/(rotation rate)$^{1/2}$ to yield i_{lim} at $S_0 = S_B$ for a range of S_B, allowing analysis by the Michaelis–Menten equation (or equivalent), as in conventional enzyme kinetics. However, note that, first, the approach to the intercept may not be truly linear due to the influence of the enzyme kinetics [52], and second, that evaluation of kinetic parameters such as k_2 requires knowledge of the enzyme surface coverage. Experimentally, the mass transport limit is more accessible when the amount of enzyme on the electrode surface is decreased [53] (thus slowing substrate depletion and increasing diffusion [54]). Good examples of Koutecky–Levich analyses are fumarate reduction by fumarate reductase from *E. coli* [18], H_2O_2 reduction by yeast C*c*P [28], and nitrite and hydroxylamine reduction by cytochrome *c* nitrite reductase from *E. coli* [55]. Importantly, although Koutecky–Levich analysis does not exploit the potential domain, analysing the reaction via the limiting current confirms that IET does not influence the rate of turnover. Thus, rates of turnover observed in PFV may be significantly faster than their equivalent in solution, which are limited by reaction with an artificial redox partner (see for example [56]).

7. An alternative model for interfacial electron transfer: systems which do not exhibit i_{lim}

The experimental data sets described above (exhibiting sigmoidal waveshapes with true limiting currents) are relatively unusual. More commonly, to a lesser or greater degree, catalytic waves continue to increase in current over significantly greater regions of potential than expected, complicating their analysis. The best-characterised example is H_2 oxidation by the NiFe hydrogenase from *Allochromatium vinosum* (*Av*H_2ase) (see Fig. 7) [57], though this phenomenon has been observed in numerous different cases [27,49,58,59]. The basic model applied to *Av*H_2ase assumes (as for succinate oxidation by fumarate reductase described above) that mass transport of the substrate (H_2) and product (H^+), and their binding and dissociation to/from the enzyme, are fast enough with respect to the catalytic transformation that they are able to maintain a pre-equilibrium (equivalent to Michaelis–Menten kinetics ($K_M = K_D$)). Even taking into account the small size and simplicity of H_2 and H^+ this assumption should be questioned for an enzyme with such a high turnover rate (estimated at >6000 s^{-1} for H_2 oxidation [53]). However, the point of interest here is that the catalytic waves from *Av*H_2ase are far from sigmoidal, and they do not reach a limiting current within the accessible potential window (see Fig. 7). The elegant explanation proposed by Léger and coworkers was that a distribution in the IET rate constant exists, perhaps due to

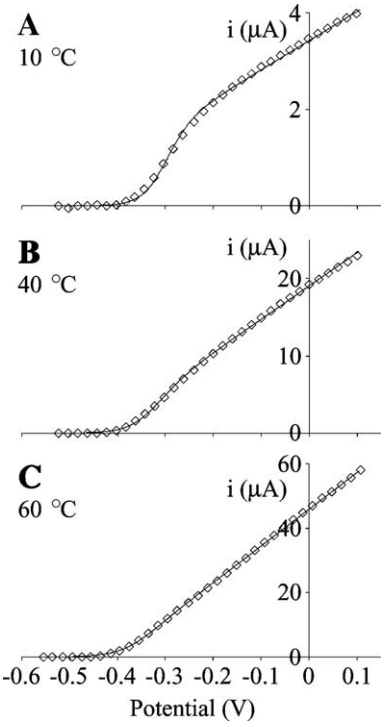

Fig. 7. Catalytic waveshapes for H_2 oxidation by the NiFe hydrogenase from *Allochromatium vinosum* modelled using a dispersion of interfacial electron transfer rate constants [57]. Background subtracted voltammograms are presented at three different temperatures, along with the modelled lines (see text). Data provided by Prof. F. A. Armstrong, Oxford University.

different orientations of the protein on the surface [57], and IET is slow enough to influence the rate of turnover. Thus, the rate of catalysis is obtained by summing the turnover rates of molecules with different IET rate constants, combined with the probability of a particular rate constant occurring. The relatively simple equation for an enzyme with an active site with three possible oxidation states (reduced and intermediate convert at E_1 and oxidised and intermediate at E_2), a rate of substrate conversion k_2 (s^{-1}), and only one orientation (a single k_0 (s^{-1}), with the rate of IET set by the Butler–Volmer equation) is given in Eq. (15) [57] (see Eq. (12) for definition of ε).

$$i = \frac{i_{\lim}}{\varepsilon_2(1+\varepsilon_1) + \frac{k_2}{k_0}\{\sqrt{\varepsilon}_1 + \sqrt{\varepsilon}_2(1+\sqrt{\varepsilon}_1)\} + 1} \tag{15}$$

In the case of a distribution in k_0 Eq. (15) is integrated over k_0 to give Eq. (16) (see [57] for details), which was used to model the data in Fig. 7 by assuming that $E_1 = E_2$.

$$i = \frac{i_{\lim}}{a}\left(1 + \frac{1}{\beta d_0}\ln\frac{a+b}{a+be^{\beta d_0}}\right) \text{ where}$$
$$a = 1 + \varepsilon_2(1+\varepsilon_1) \text{ and}$$
$$b = \frac{k_2}{k_0^{\max}}\left\{\sqrt{\varepsilon}_1 + \sqrt{\varepsilon}_2(1+\varepsilon_1)\right\} \tag{16}$$

In Eq. (16), βd_0 is the electron transfer decay constant multiplied by the diameter of the active surface of a spherical enzyme, and $k_0^{\max}$ is the rate of IET at the point of closest approach between enzyme cofactor and surface. Note that in Fig. 7, the waveshape deviates most from sigmoidal at high temperature, as k_2 increases with temperature but k_0 is temperature independent (consistent with the idea that non-sigmoidal waveshapes are observed when turnover is fast with respect to electron transfer). This model has been applied to characterising the active site of *Av*H_2ase in some detail [60]. However, it is important to note that although considering a distribution in the IET rate constant has by now allowed accurate modelling of the complex voltammetry of several enzymes, the underlying physical basis of the model remains unsubstantiated.

8. Comprehensive models for steady-state catalysis which consider interfacial electron transport, enzyme turnover and mass transport

A typical enzyme does not obey simple Michaelis–Menten kinetics, because the rate of substrate binding influences the rate of catalysis, and does not have such a slow rate of turnover (or a substrate with such a high diffusion coefficient) that mass transport can be ignored. Scheme 2B shows the simplest general scheme, though of course more complex schemes are easily envisaged (for example, including the binding of substrate to alternative oxidation states). Mathematically, Scheme 2B can be expressed and solved by using the steady-state approximation for each intermediate enzyme species (applying the Michaelis–Menten and Butler–Volmer equations) to give the rate of enzyme turnover (V) as a function of potential (Eq. (17)) [52].

$$V = \frac{k_2\Gamma_{\text{Total}}}{1 + \frac{K_m}{S_0}(1+\varepsilon_2+\varepsilon_1\varepsilon_2) + \frac{k_2}{k_0}(\sqrt{\varepsilon}_1 + \sqrt{\varepsilon}_2(1+\varepsilon_1))} \tag{17}$$

The rate of enzyme turnover is the rate of substrate depletion and, at steady-state, it is equal to the rate of supply by mass transport. Thus, Eq. (17) is equated to the Levich equation (Eq. (13)), solved for S_0, and then S_0 is resubstituted to give the current as a function of potential (Eq. (18)).

$$i = \frac{nFA\Gamma_{\text{Total}}k_2}{1 + k_2b/k_0 + 2K_m a/S_B\left(c + \sqrt{(c^2 + 4K_m a/[S_B(1+k_2b/k_0)])}\right)^{-1}}$$

where

$$c = 1 - \frac{K_m m_0 a + k_2 C_{\text{Total}}}{S_B m_0(1 + k_2 b/k_0)} \tag{18}$$

Alternatively, Eq. (17) can be integrated to conform to a dispersion of IET rate constants and then equated to the rate of mass transport to give Eq. (19):

$$m_0(S_B - S_0) = \frac{k_2\Gamma_{\text{Total}}}{\beta d_0(1 + aK_m/S_0)}\ln\left[\frac{(1+aK_m/S_0)k_0^{\max} + k_2b}{(1+aK_m/S_0)k_0^{\min} + k_2b}\right] \tag{19}$$

Eq. (19) must be solved numerically to produce S_0, and then the current can be calculated at each potential from Eq. (13) as above [61].

Fig. 8 shows example voltammograms recorded for NADH oxidation by the hydrophilic subcomplex of NADH:ubiquinone oxidoreductase (complex I), and fitted using Eq. (19) [61]. Also shown are matching profiles for the surface concentration of substrate, showing that S_0 decreases significantly below S_B, even at the highest S_B and highest rotation rate. Thus, although Eq. (19) is highly complex it provides further theoretical basis for interpreting and understanding voltammograms which do not conform to the ideal sigmoidal shapes predicted by classical electrochemistry.

To conclude this part of the discussion of catalytic voltammetry, Table 1 summarises the essential characteristics of each model discussed.

9. Unusual catalytic waveforms

Fascinating new insights into enzyme catalysis are revealed by PFV under conditions when the enzyme itself controls the rate of catalysis, when voltammograms deviate spectacularly from the basic sigmoidal waveshape. Thus, they reveal the presence of different forms of the enzyme, with varying catalytic abilities, which prevail at different potentials [62]. The first reported example was from succinate dehydrogenase, the hydrophilic domain of succinate:ubiquinone oxidoreductase from bovine heart mitochondria [63]. When the enzyme is catalysing fumarate reduction the

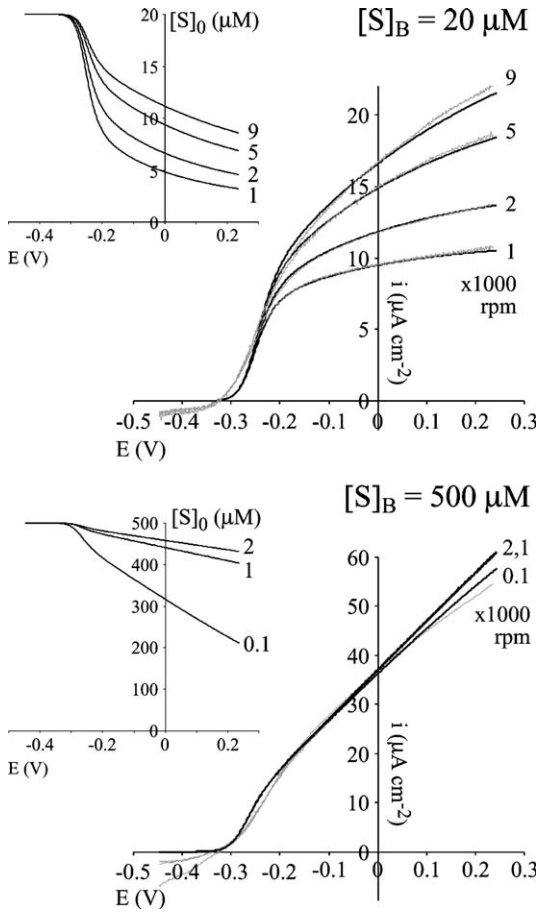

Fig. 8. Electrocatalytic oxidation of NADH by subcomplex Iλ from complex I from bovine heart mitochondria [61]. The protein was co-adsorbed with DDAB on a PGE electrode, and background subtracted voltammograms are reported over a range of rotation rates at two different NADH concentrations. Experimentally recorded voltammograms are in grey, modelled voltammograms (black) were calculated as described in the text. Inset: substrate concentration at the electrode surface as a function of potential, corresponding to each voltammogram. Experimental conditions: 25 mV s^{-1}, 30 °C, 10 mM KCl +mixed buffer, pH 7.8.

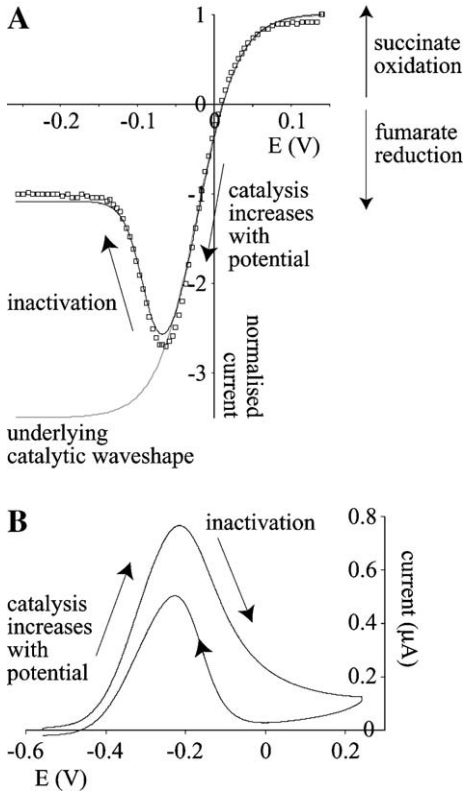

Fig. 9. Catalytic voltammograms showing potential induced conversions between different enzyme states with different catalytic activities. (A) The interconversion of succinate and fumarate by succinate dehydrogenase from bovine heart mitochondria [48]. At positive potentials, the enzyme catalyses succinate oxidation, at negative potentials fumarate reduction. The succinate oxidation wave is sigmoidal, but the fumarate reduction wave shows a maximum activity at intermediate potential, showing that the enzyme converts to a less active form. Conditions: pH 7.0, 38 °C, 10 mV s^{-1}, 500 rpm, [succinate]=[fumarate]=0.13 mM. (B) Conversion between active and inactive forms of *Allochromatium vinosum* hydrogenase, visualised by the oxidation of 1 bar H_2. Conditions: pH 8.8, 48 °C, 0.3 mV s^{-1}, 2500 rpm [67]. The data used to make panel B were provided by Prof. F. A. Armstrong, Oxford University.

optimum activity (in either scan direction) occurs at intermediate driving force—a region of potential exists where the activity decreases as the driving force is increased (see Fig. 9A). In the case of succinate dehydrogenase the potential of the 'switch' corresponds roughly to that of the FAD in the enzyme's active site [48], though a molecular explanation of the effect remains elusive. In the related enzyme, fumarate reductase from *E. coli*, the waveshape also deviates from a basic sigmoid, except that in this case the

Table 1
Summary of the models described for the interpretation of electrocatalytic voltammetry

	Mass transport	Interfacial electron transport	Enzyme kinetics	Comments	References
Succinate oxidation by fumarate reductase	Fast	Fast	Pre-equilibrium binding, k_2 limiting	Redox titration of active site amplified by catalysis	[41]
Variation of limiting current	Levich	Fast	Michaelis–Menten equation	Analogous to conventional enzyme kinetics	[18,28,55]
H_2 oxidation by NiFe hydrogenase	Fast	Butler–Volmer Dispersion	Pre-equilibrium binding, k_2 limiting	Physical explanation for non sigmoidal waveshapes	[57]
Basic complete model (Eq. (18))	Levich	Butler–Volmer (homogeneous)	Michaelis–Menten equation	Basis for understanding substrate concentration and rotation rate dependence of complete waveshape	[52]
NADH oxidation by subcomplex Iλ	Levich	Butler–Volmer Dispersion	Michaelis–Menten equation	Incorporates all three rate limiting processes	[61]

current is 'boosted', not shut down, as the driving force for fumarate reduction is increased [15,18]. The potential of the boost corresponds to the potential of the second of three iron–sulphur clusters which form a chain through the enzyme (see Scheme 1), the low-potential [4Fe–4S] cluster. In addition, the oxidation state of the [4Fe–4S] cluster determines the rate of release of an inhibitor, oxaloacetate, from the FAD active site. Thus, although the cluster is distant (ca. 20 Å away) from the active site it strongly influences the reactions occurring there [19]. The decahaem enzyme cytochrome *c* nitrite reductase is another, unrelated, enzyme which exhibits both a potential optimum for catalysis and potential dependent inhibitor binding [55,64]. Potential optima have been observed also in molybdenum enzymes, in DMSO reductase [65] and nitrate reductase [58,59,62]. In DMSO reductase the optimal potentials for DMSO reduction and trimethylphosphine oxidation coincide, and the potential of optimal activity was correlated to the potential at which the Mo is held in the Mo(V) state.

In all these cases, conversion between 'active' and 'less-active' enzyme forms is rapid on the experimental timescale, and so the state of the enzyme is independent of scan direction and starting potential. In contrast, conversion between the active and inactive states of NiFe hydrogenases, under anaerobic conditions, is slow [66,67]. If a catalytic voltammogram for H_2 oxidation is recorded from the low potential limit, at 'normal' scan rate, then a typical sigmoidal voltammogram is observed [56]. This is because the enzyme is in the active state at negative potential, and conversion to the inactive state, which occurs at more positive potential, is slow and does not occur significantly during the scan. However, if the potential is cycled very slowly (Fig. 9B, 0.3 mV s^{-1}) then a reversible transition occurs, with the amount of active enzyme present defined by the magnitude of the catalytic current [67]. Indeed, conversions between the different states are so slow that they are best studied using potential step experiments, in which the 'relaxation' of the system following a large jump in potential is monitored via changes in the rate of catalysis, or by following the response of the current (at a single potential) to the addition of molecules such as O_2 or CO [68,69]. Thus, the ability of PFV to control the potential domain and define the status of the enzyme has proved instrumental in untangling the complex reactions that define the catalytic activity of hydrogenase enzymes [66].

10. Concluding remarks

It is clear that protein film voltammetry is capable of providing new and detailed information on the mechanisms of redox enzymes and proteins. However, considerable challenges exist—in creating a suitable interface to adsorb the protein in a native state and in electrical contact with the electrode, in designing appropriate experiments to interrogate the reaction of interest, and in understanding and interpreting voltammetric results on both a qualitative and quantitative level. It is hoped that this review will aid the fulfillment of these aims, and promote the application and development of protein film voltammetry as a technique in both basic and applied science.

Acknowledgements

I thank Professor Fraser Armstrong, Oxford University, for generously providing data which is included in (Figs. 2, 3, 5–7, and 9. Research in the author's laboratory is funded by The Medical Research Council.

References

[1] F.A. Armstrong, H.A. Heering, J. Hirst, Reactions of complex metalloproteins studied by protein-film voltammetry, Chem. Soc. Rev. 26 (1997) 169–179.
[2] C. Léger, S.J. Elliott, K.R. Hoke, L.J.C. Jeuken, A.K. Jones, F.A. Armstrong, Enzyme electrokinetics: using protein film voltammetry to investigate redox enzymes and their mechanisms, Biochemistry 42 (2003) 8653–8662.
[3] F.A. Armstrong, Recent developments in dynamic electrochemical studies of adsorbed enzymes and their active sites, Curr. Opin. Chem. Biol. 9 (2005) 110–117.
[4] F.A. Armstrong, G.S. Wilson, Recent developments in Faradaic bioelectrochemistry, Electrochim. Acta 45 (2000) 2623–2645.
[5] J.F. Rusling, Enzyme bioelectrochemistry in cast biomembrane-like films, Acc. Chem. Res. 31 (1998) 363–369.
[6] F.A. Armstrong, J.N. Butt, A. Sucheta, Voltammetric studies of redox-active centers in metalloproteins adsorbed on electrodes, Methods Enzymol. 227 (1993) 479–500.
[7] J. Hirst, F.A. Armstrong, Fast-scan cyclic voltammetry of protein films on pyrolytic graphite edge electrodes: characteristics of electron exchange, Anal. Chem. 70 (1998) 5062–5071.
[8] L.J.C. Jeuken, F.A. Armstrong, Electrochemical origins of hysteresis in the electron-transfer reactions of adsorbed proteins: contrasting behavior of the "blue" copper protein, azurin, adsorbed on pyrolytic graphite and modified gold electrodes, J. Phys. Chem., B 105 (2001) 5271–5282.
[9] R.A. Marcus, Electron transfer reactions in chemistry—theory and experiment (Nobel lecture), Angew. Chem., Int. Ed. Engl. 32 (1993) 1111–1121.
[10] A.J. Bard, L.R. Faulkner, Electrochemical methods, 2nd Ed.Wiley, New York, 2001.
[11] Y. Zu, J.A. Fee, J. Hirst, Complete thermodynamic characterisation of reduction and protonation of the bc_1-type Rieske [2Fe–2S] center of *Thermus thermophilus*, J. Am. Chem. Soc. 123 (2001) 9906–9907.
[12] E. Laviron, General expression of the linear potential sweep voltammogram in the case of diffusionless electrochemical systems, J. Electroanal. Chem. 101 (1979) 19–28.
[13] V. Massey, Activation of molecular oxygen by flavins and flavoproteins, J. Biol. Chem. 269 (1994) 22459–22462.
[14] W.M. Clark, Oxidation–reduction potentials of organic systems, The Williams and Wilkins Company, Baltimore, 1960.
[15] H.A. Heering, J.H. Weiner, F.A. Armstrong, Direct detection and measurement of electron relays in a multicentered enzyme: voltammetry of electrode-surface films of *E. coli* fumarate reductase, an iron–sulfur flavoprotein, J. Am. Chem. Soc. 119 (1997) 11628–11638.
[16] Y. Zu, S. di Bernardo, T. Yagi, J. Hirst, Redox properties of the [2Fe–2S] center in the 24 kDa (NQO2) subunit of NADH:ubiquinone oxidoreductase (complex I), Biochemistry 41 (2002) 10056–10069.
[17] T.M. Iverson, C. Luna-Chavez, G. Cecchini, D.C. Rees, Structure of the *Escherichia coli* fumarate reductase respiratory complex, Science 284 (1999) 1961–1966.
[18] A. Sucheta, R. Cammack, J. Weiner, F.A. Armstrong, Reversible electrochemistry of fumarate reductase immobilized on an electrode surface. Direct voltammetric observations of redox centers and their

participation in rapid catalytic electron transport, Biochemistry 32 (1993) 5455–5465.
[19] J.M. Hudson, K. Heffron, V. Kotlyar, Y. Sher, E. Maklashina, G. Cecchini, F.A. Armstrong, Electron transfer and catalytic control by the iron–sulfur clusters in a respiratory enzyme, *E. coli* fumarate reductase, J. Am. Chem. Soc. 127 (2005) 6977–6989.
[20] J.N. Butt, S.E.J. Fawcett, J. Breton, A.J. Thomson, F.A. Armstrong, Electrochemical potential and pH dependences of [3Fe–4S] to [M3Fe–4S] cluster transformations (M=Fe, Zn, Co and Cd) in ferredoxin III from *Desulfovibrio africanus* and detection of a cluster with M=Pb, J. Am. Chem. Soc. 119 (1997) 9729–9737.
[21] K. Chen, C.A. Bonagura, G.J. Tilley, J.P. McEvoy, Y.S. Jung, F.A. Armstrong, C.D. Stout, B.K. Burgess, Crystal structures of ferredoxin variants exhibiting large changes in [Fe–S] reduction potential, Nat. Struct. Biol. 9 (2002) 188–192.
[22] Y. Zu, M.M.-J. Couture, D.R.J. Kolling, A.R. Crofts, L.D. Eltis, J.A. Fee, J. Hirst, Reduction potentials of Rieske clusters: importance of the coupling between oxidation state and histidine protonation state, Biochemistry 42 (2003) 12400–12408.
[23] L.J.C. Jeuken, P. van Vliet, M.P. Verbeet, R. Camba, J.P. McEvoy, F.A. Armstrong, G.W. Canters, Role of the surface-exposed and copper-coordinating histidine in blue copper proteins: the electron-transfer and redox-coupled ligand binding properties of His117Gly azurin, J. Am. Chem. Soc. 122 (2000) 12186–12194.
[24] C.R. Hess, G.A. Juda, D.M. Dooley, R.N. Amii, M.G. Hill, J.R. Winkler, H.B. Gray, Gold electrodes wired for coupling with the deeply buried active site of *Arthrobacter globiformis* amine oxidase, J. Am. Chem. Soc. 125 (2003) 7156–7157.
[25] K. Fujita, N. Nakamura, H. Ohno, B.S. Leigh, K. Niki, H.B. Gray, J.H. Richards, Mimicking protein–protein electron transfer: voltammetry of *Pseudomonas aeruginosa* azurin and the *Thermus thermophilus* Cu_A domain at derivatized self-assembled monolayer gold electrodes, J. Am. Chem. Soc. 126 (2004) 13954–13961.
[26] K.-F. Aguey-Zinsou, P.V. Bernhardt, U. Kappler, A.G. McEwan, Direct electrochemistry of a bacterial sulfite dehydrogenase, J. Am. Chem. Soc. 125 (2003) 530–535.
[27] K.R. Hoke, N. Cobb, F.A. Armstrong, R. Hille, Electrochemical studies of arsenite oxidase: an unusual example of a highly cooperative two-electron molybdenum centre, Biochemistry 43 (2004) 1667–1674.
[28] M.S. Mondal, H.A. Fuller, F.A. Armstrong, Direct measurement of the reduction potential of catalytically active cytochrome *c* peroxidase compound I: voltammetric detection of a reversible, cooperative two-electron transfer reaction, J. Am. Chem. Soc. 118 (1996) 263–264.
[29] A. El Kasmi, J.M. Wallace, E.F. Bowden, S.M. Binet, R.J. Linderman, Controlling interfacial electron-transfer kinetics of cytochrome *c* with mixed self-assembled monolayers, J. Am. Chem. Soc. 120 (1998) 225–226.
[30] K.L. Turner, M.K. Doherty, H.A. Heering, F.A. Armstrong, G.A. Reid, S. K. Chapman, Redox properties of flavocytochrome c_3 from *Shewanella frigidimarina* NCIMB400, Biochemistry 38 (1999) 3302–3309.
[31] H.A. Heering, F.G.M. Wiertz, C. Dekker, S. de Vries, Direct immobilization of native yeast iso-1 cytochrome *c* on bare gold: fast electron relay to redox enzymes and zeptomole protein film voltammetry, J. Am. Chem. Soc. 126 (2004) 11103–11112.
[32] J.L.C. Duff, J.L.J. Breton, J.N. Butt, F.A. Armstrong, A.J. Thomson, Novel redox chemistry of [3Fe–4S] Clusters: electrochemical characterization of the all-Fe(II) form of the [3Fe–4S] cluster generated reversibly in various proteins and its spectroscopic investigation in *Sulfolobus acidocaldarius* ferredoxin, J. Am. Chem. Soc. 118 (1996) 8593–8603.
[33] E.J. Leggate, E. Bill, T. Essigke, G.M. Ullmann, J. Hirst, Formation and characterisation of an all-ferrous Rieske cluster and stabilization of the $[2Fe–2S]^0$ core by protonation, Proc. Natl. Acad. Sci. U. S. A. 101 (2004) 10913–10918.
[34] E.J. Leggate, J. Hirst, Roles of the disulphide bond and adjacent residues in determining the reduction potentials and stabilities of respiratory-type Rieske clusters, Biochemistry 44 (2005) 7048–7058.
[35] E.A. Berry, M. Guergova-Kuras, L.-S. Huang, A.R. Crofts, Structure and function of cytochrome *bc* complexes, Annu. Rev. Biochem. 69 (2000) 1005–1075.
[36] Y. Zu, J.A. Fee, J. Hirst, Breaking and reforming the disulfide bond at the high-potential, respiratory-type [2Fe–2S] center of *Thermus thermophilus*: characterisation of the sulfyhydryl state by protein-film voltammetry, Biochemistry 41 (2002) 14054–14065.
[37] B. Shen, L.L. Martin, J.N. Butt, F.A. Armstrong, C.D. Stout, G.M. Jensen, P.J. Stephens, G.N. La Mar, C.M. Gorst, B.K. Burgess, *Azotobacter vinelandii* ferredoxin I: aspartate 15 facilitates proton transfer to the reduced [3Fe–4S] cluster, J. Biol. Chem. 268 (1993) 25928–25939.
[38] J.N. Butt, A. Sucheta, L.L. Martin, B. Shen, B.K. Burgess, F.A. Armstrong, Voltammetric study of proton-gated electron transfer in a mutant ferredoxin. Altering aspartate to asparagine blocks oxidation of the [3Fe–4S] cluster of *Azotobacter vinelandii* ferredoxin I, J. Am. Chem. Soc. 115 (1993) 12587–12588.
[39] F.A. Armstrong, Evaluations of reduction potential data in relation to coupling, kinetics and function, J. Biol. Inorg. Chem. 2 (1997) 139–142.
[40] F.A. Armstrong, R. Camba, H.A. Heering, J. Hirst, L.J.C. Jeuken, A.K. Jones, C. Léger, J.P. McEvoy, Fast voltammetric studies of the kinetics and energetics of coupled electron-transfer reactions in proteins, Faraday Discuss. 116 (2000) 191–203.
[41] C. Léger, K. Heffron, H.R. Pershad, E. Maklashina, C. Luna-Chavez, G. Cecchini, B.A.C. Ackrell, F.A. Armstrong, Enzyme electrokinetics: energetics of succinate oxidation by fumarate reductase and succinate dehydrogenase, Biochemistry 40 (2001) 11234–11245.
[42] A.K. Jones, R. Camba, G.A. Reid, S.K. Chapman, F.A. Armstrong, Interruption and time-resolution of catalysis by a flavoenzyme using fast scan protein film voltammetry, J. Am. Chem. Soc. 122 (2000) 6494–6495.
[43] J.N. Butt, A. Sucheta, F.A. Armstrong, J. Breton, A.J. Thomson, E.C. Hatchikian, Voltammetric characterization of rapid and reversible binding of an exogeous thiolate ligand at a [4Fe–4S] cluster in Ferredoxin III from *Desulfovibrio africanus*, J. Am. Chem. Soc. 115 (1993) 1413–1421.
[44] R. Camba, F.A. Armstrong, Investigations of the oxidative disassembly of Fe–S clusters in *Clostridium pasteurianum* 8Fe ferredoxin using pulsed protein-film voltammetry, Biochemistry 39 (2000) 10587–10598.
[45] J.N. Butt, F.A. Armstrong, J. Breton, S.J. George, A.J. Thomson, C.E. Hatchikian, Investigation of metal ion uptake reactivities of [3Fe–4S] clusters in proteins: voltammetry of co-adsorbed ferredoxin-aminocyclitol films at graphite electrodes and spectroscopic identification of transformed clusters, J. Am. Chem. Soc. 113 (1991) 6663–6670.
[46] J. Hirst, J.L.C. Duff, G.N.L. Jameson, M.A. Kemper, B.K. Burgess, F.A. Armstrong, Kinetics and mechanism of redox-coupled, long-range proton transfer in an iron–sulfur protein. Investigation by fast-scan protein-film voltammetry, J. Am. Chem. Soc. 120 (1998) 7085–7094.
[47] K.S. Chen, J. Hirst, R. Camba, C.A. Bonagura, C.D. Stout, B.K. Burgess, F.A. Armstrong, Atomically defined mechanism for proton transfer to a buried redox centre in a protein, Nature 405 (2000) 814–817.
[48] J. Hirst, A. Sucheta, B.A.C. Ackrell, F.A. Armstrong, Electrocatalytic voltammetry of succinate dehydrogenase: direct quantification of the catalytic properties of a complex electron-transport enzyme, J. Am. Chem. Soc. 118 (1996) 5031–5038.
[49] Y. Zu, R.J. Shannon, J. Hirst, Reversible, electrochemical interconversion of NADH and NAD^+ by the catalytic (Iλ) subcomplex of mitochondrial NADH: ubiquinone oxidoreductase (complex I), J. Am. Chem. Soc. 125 (2003) 6020–6021.
[50] J. Hirst, B.A.C. Ackrell, F.A. Armstrong, Global observation of hydrogen/deuterium isotope effects on bidirectional catalytic electron transport in an enzyme: direct measurement by protein-film voltammetry, J. Am. Chem. Soc. 119 (1997) 7434–7439.
[51] I.H. Segel, Enzyme kinetics. Behavior and analysis of rapid equilibrium and steady-state enzyme systems, Wiley, 1975.
[52] H.A. Heering, J. Hirst, F.A. Armstrong, Interpreting the catalytic voltammetry of electroactive enzymes adsorbed on electrodes, J. Phys. Chem., B 102 (1998) 6889–6902.
[53] A.K. Jones, E. Sillery, S.P.J. Albracht, F.A. Armstrong, Direct comparison of the electrocatalytic oxidation of hydrogen by an enzyme and a platinum catalyst, Chem. Commun. (2002) 866–867.

[54] F.A. Armstrong, A.M. Bond, F.N. Büchi, A. Hamnett, H.A.O. Hill, A.M. Lannon, O.C. Lettington, C.G. Zoski, Electrocatalytic reduction of hydrogen peroxide at a stationary pyrolytic graphite electrode surface in the presence of cytochrome *c* peroxidase: a description based on a microelectrode array model for adsorbed enzyme molecules, Analyst 118 (1993) 973–978.

[55] H.C. Angove, J.A. Cole, D.J. Richardson, J.N. Butt, Protein film voltammetry reveals distinctive fingerprints of nitrite and hydroxylamine by a cytochrome *c* nitrite reductase, J. Biol. Chem. 277 (2002) 23374–23381.

[56] H.R. Pershad, J.L.C. Duff, H.A. Heering, E.C. Duin, S.P.J. Albracht, F.A. Armstrong, Catalytic electron transport in *Chromatium vinosum* [NiFe]-hydrogenase: application of voltammetry in detecting redox-active centers and establishing that hydrogen oxidation is very fast even at potentials close to the reversible H^+/H_2 value, Biochemistry 38 (1999) 8992–8999.

[57] C. Léger, A.K. Jones, S.P.J. Albracht, F.A. Armstrong, Effect of a dispersion of interfacial electron transfer rates on steady-state catalytic electron transport in [NiFe]-hydrogenase and other enzymes, J. Phys. Chem., B 106 (2002) 13058–13063.

[58] L.J. Anderson, D.J. Richardson, J.N. Butt, Catalytic protein film voltammetry from a respiratory nitrate reductase provides evidence for complex electrochemical modulation of enzyme activity, Biochemistry 40 (2001) 11294–11307.

[59] B.J.N. Jepson, L.J. Anderson, L.M. Rubio, C.J. Taylor, C.S. Butler, E. Flores, A. Herrero, J.N. Butt, D.J. Richardson, Tuning a nitrate reductase for function, J. Biol. Chem. 279 (2004) 32212–32218.

[60] C. Léger, A.K. Jones, W. Roseboom, S.P.J. Albracht, F.A. Armstrong, Enzyme electrokinetics: hydrogen evolution and oxidation by *Allochromatium vinosum* NiFe hydrogenase, Biochemistry 41 (2002) 15736–15746.

[61] T. Reda, J. Hirst, Interpreting the catalytic voltammetry of an adsorbed enzyme by considering substrate mass transfer, enzyme turnover, and interfacial electron transport, J. Phys. Chem., B 110 (2006) 1394–1404.

[62] S.J. Elliott, K.R. Hoke, K. Heffron, M. Palak, R.A. Rothery, J.H. Weiner, F. A. Armstrong, Voltammetric studies of the catalytic mechanism of the respiratory nitrate reductase from *Escherichia coli*: how nitrate reduction and inhibition depend on the oxidation state of the active site, Biochemistry 43 (2004) 799–807.

[63] A. Sucheta, B.A.C. Ackrell, B. Cochran, F.A. Armstrong, Diode-like behaviour of a mitochondrial electron-transport enzyme, Nature 356 (1992) 361–362.

[64] J.D. Gwyer, D.J. Richardson, J.N. Butt, Resolving complexity in the interactions of redox enzymes and their inhibitors: contrasting mechanisms for the inhibition of a cytochrome *c* nitrite reductase revealed by protein film voltammetry, Biochemistry 43 (2004) 15086–15094.

[65] K. Heffron, C. Léger, R.A. Rothery, J.H. Weiner, F.A. Armstrong, Determination of an optimal potential window for catalysis by *E. coli* dimethyl sulfoxide reductase and hypothesis on the role of Mo (V) in the reaction pathway, Biochemistry 40 (2001) 3117–3126.

[66] F.A. Armstrong, Hydrogenases: active site puzzles and progress, Curr. Opin. Chem. Biol. 8 (2004) 133–140.

[67] A.K. Jones, S.E. Lamle, H.R. Pershad, K.A. Vincent, S.P.J. Albracht, F.A. Armstrong, Enzyme electrokinetics: electrochemical studies of the anaerobic interconversions between active and inactive states of *Allochromatium vinosum* [NiFe]-hydrogenase, J. Am. Chem. Soc. 125 (2003) 8505–8514.

[68] S.E. Lamle, S.P.J. Albracht, F.A. Armstrong, Electrochemical potential-step investigations of the aerobic interconversions of [NiFe]-hydrogenase from *Allochromatium vinosum*: insights into the puzzling difference between unready and ready oxidized inactive states, J. Am. Chem. Soc. 126 (2004) 14899–14909.

[69] S.E. Lamle, S.P.J. Albracht, F.A. Armstrong, The mechanism of activation of a NiFe-hydrogenase by electrons, hydrogen and carbon monoxide, J. Am. Chem. Soc. 127 (2005) 6595–6604.

[70] J.M. Hudson, D. Phil. Thesis, University of Oxford (2005).